One-, two-, and three-dimensional root water uptake functions for transient modeling

J. A. Vrugt and M. T. van Wijk

Institute for Biodiversity and Ecosystem Dynamics, University of Amsterdam, Amsterdam, Netherlands

J. W. Hopmans

Hydrology Program, Department of Land, Air and Water Resources (LAWR), University of California
Davis, California, USA

J. Šimunek

U.S. Department of Agriculture Salinity Laboratory, University of California, Riverside, California, USA

Abstract. Although solutions of multidimensional transient water flow can be obtained by numerical modeling, their application may be limited as root water uptake is generally considered to be one- or two-dimensional only. This is especially the case for trees. The first objective of this paper is to test the suitability of a three-dimensional root water uptake model for the simultaneous simulation of transient soil water flow around an almond tree. The soil hydraulic and root water uptake parameters were optimized by minimizing the residuals between measured and simulated water content data. Water content was measured in a three-dimensional grid around a sprinkler-irrigated almond tree for a 16 day period, following irrigation. A second objective was to compare the performance and results of the three-dimensional flow model with one- and two-dimensional root water uptake models. For this purpose, measured water contents were aggregated in the x and y direction in the one-dimensional case and in the radial direction for the two-dimensional uptake model. For the estimation of root water uptake model parameters a genetic algorithm was used to estimate the approximate global minimum of the parameter space, whereas final parameters were determined using the Simplex optimization algorithm. With the optimized root water uptake parameters, simulated and measured water contents during the 16-day period were in excellent agreement for all root water uptake models. Most significantly, the spatial variation in flux density below the rooting zone decreased when reducing multidimensional root water uptake to fewer dimensions, thereby justifying the proposed multidimensional approach.

1. Introduction

From a hydrological perspective, water uptake by root systems and their spatial distribution may exert a large degree of control on the water fluxes to the atmosphere and the groundwater [*Canadell et al.*, 1996]. For an improved understanding of the magnitude of these fluxes, accurate estimates of the temporal and spatial root water uptake patterns are needed. Clearly, quantification of root water extraction rates also contributes to an understanding of chemical fluxes in the vadose zone in both ecological and hydrological studies [*Somma et al.*, 1998] as well as their control by vegetation. Interactions between roots and soil in the rhizosphere influence the quality and quantity of water transported in and exported from the vadose zone. An understanding of the interactions between the roots and surrounding soil and solutes under a variety of changing environmental conditions has large implications since it will lead to a decrease in contamination of subsurface and surface water resources by reducing the loss of fertilizers and other agrochemicals below the root zone [*Clausnitzer and Hopmans*, 1994; *Clothier and Green*, 1994]. Moreover, the rhizos-

phere might be responsible for accelerated breakdown of organic chemicals by biodegradation [*Walton and Anderson*, 1990] and phytoremediation [*Nyer and Gatliff*, 1996]; hence a thorough understanding of root function regarding uptake of water and associated solutes is warranted.

Actual root water uptake spatially depends not only on the root density distribution but also on its temporal functioning as determined by soil water availability and soil salinity. In addition to water stress in periods of low water availability, root water uptake is also reduced when concentrations of soluble salts exceed plant-specific threshold values [*Homae*, 1999]. In irrigated soils, particularly in arid and semiarid regions, plants are generally subjected to both salinity and water stress. In these regions, soil and water management practices are based on maintaining a favorable soil water content and salinity status in the root zone, thereby minimizing periods of water stress while controlling leaching to minimize salinity stress.

The influence of plant root systems on water and chemical movement can be better understood using soil water simulation models, provided that accurate spatial and temporal root water uptake distributions are included [*Musters and Bouten*, 1999]. One of the earliest detailed quantitative studies of water extraction by a plant root was presented by *Gardner* [1960]. This microscopic model considered a single root to be equiv-

alent to an infinitely long cylinder of uniform radius with water-absorbing properties. The steady state soil water flow equation was solved analytically assuming radial flow and imposed root water uptake rates. Soil water matric head distributions around the idealized root were calculated. This concept was extended in later papers [*Gardner*, 1964, 1965; *Gardner and Ehlig*, 1962] and proved to be very insightful but lacked practical applicability since the detailed geometry of the rooting system is difficult to measure and is time dependent. Consequently, most root water extraction terms have been developed using a macroscopic rather than a microscopic approach. Nonetheless, all macroscopic models preserve the essence of *Gardner*'s [1960] insight.

In the macroscopic approach of Richards' equation a sink term representing the water extraction of the entire root system is included to describe transient multidimensional water flow [*Whisler et al.*, 1968; *Molz and Remson*, 1970; *Clausnitzer and Hopmans*, 1994], according to

$$\frac{\partial \theta}{\partial t} = \nabla \cdot [\mathbf{K} \nabla (h - z)] - S(x, y, z, t), \quad (1)$$

where θ is the volumetric water content ($L^3 L^{-3}$), $\mathbf{K}$ is the unsaturated hydraulic conductivity tensor ($L T^1$), h (L) is the soil water matric head, z (L) is the depth which is included for vertical flow only, and S is the volumetric sink term ($L^3 L^{-3} T^{-1}$), representing root water uptake as a function of both space and time. The benefits of such an approach are evident since it allows direct integration of root water uptake with transient soil water flow and provides natural interactions between transpiration and root water extraction, that is, as long as we know the mechanisms with which to describe S.

Though transient soil water flow in the vadose zone is often simulated in one, two, and three spatial dimension; root water uptake is generally considered simply to be a function of the vertical dimension only. For uniform crops with a spatially uniform water uptake pattern, one-dimensional models may suffice. However, for row crops and tree lines, for example, a two-dimensional representation would be better. For isolated trees, such as apples and almonds in large monocultures, the process of water uptake is complex, and a three-dimensional representation would therefore seem appropriate [*Green and Clothier*, 1999]. Flow models such as HYDRUS-3D, being an update of the SWMS_3D code of *Šimunek et al.* [1995], allow multidimensional root water uptake. However, spatial characterization of root water uptake data is generally lacking to support multidimensional root water uptake parameters. Moreover, available uptake models are largely limited to one dimension only [*Feddes et al.*, 1976; *Molz*, 1981; *Jarvis*, 1989] and describe variations in water uptake with soil depth while allowing for reduction in uptake by soil water stress. Exceptions are the two-dimensional models proposed by *Neuman et al.* [1975], *Warrick et al.* [1980], *Coelho and Or* [1996], and most recently, *Vrugt et al.* [2001b].

In the past few years, computing capabilities have significantly improved the effectiveness of multidimensional soil water flow models to study spatial and temporal patterns of root water uptake. Such a multidimensional approach in root water uptake is needed if uptake is varying in space, thereby allowing a more accurate quantification of spatial variability of the soil water regime, including the water and solute flux densities below the rooting zone. The objective of this study is threefold. First, we test the suitability of a three-dimensional model for the simultaneous, dynamic simulation of soil water flow and root water uptake. A three-dimensional finite element grid over the considered soil domain serves to define the spatial distribution of soil physical properties and root characteristics and acts as a framework for the transient water flow model. Soil physical and root parameters are subsequently estimated using inverse modeling while using the measured spatial distribution of water contents around a sprinkler-irrigated almond tree during a 16 day period. A second objective was to compare the results of the three-dimensional analysis with numerical models describing soil water flow and root water uptake in one and two dimensions, with uptake parameters optimized using the same field data set. Finally, the third goal of the simulation study is to evaluate the improved prediction of the spatial variability of soil water flux taking into consideration the multidimensionality of root water uptake. Whereas verification of the presented multidimensional uptake model is limited to a single data set, the main goal of this study is to emphasize the importance of multidimensional root water uptake modeling in root zone domains with spatially distributed root water uptake.

2. Materials and Methods

2.1. One-, Two-, and Three-Dimensional Root Water Uptake Model

Recently, *Vrugt et al.* [2001b] proposed a one-dimensional root water uptake model, which was shown to be very flexible. It was based on the model by *Raats* [1974]

$$\beta(z) = \left[1 - \frac{z}{Z_m} \right] e^{-(p_z/Z_m)|z^* - z|}, \quad (2)$$

where $\beta(z)$ is a shape factor describing the spatial distribution of potential root water uptake with depth, Z_m (L) is the maximum rooting depth, and p_z and z^* (L) are empirical parameters. These parameters are included to provide for zero root water uptake at $z = Z_m$ to account for asymmetrical root water uptake with depth and also to allow for a maximum root water uptake rate at any depth, $Z_0 (0 \leq Z_0 \leq Z_m)$. The asymmetry in root water uptake with soil depth is determined by the ratio between p_z for $z \leq z^*$ and the p_z value for $z > z^*$. To reduce the number of parameters, p_z is set to unity for values of $z > z^*$, whereas it is a fitted value for $z \leq z^*$. The value of Z_0, the depth of maximum uptake, can simply be calculated from the first derivative, or

$$\left. \frac{d\beta(z)}{dz} \right|_{z_0} = 0.$$

Assuming axial symmetry in root water uptake while using the same root water uptake model leads to the following two-dimensional root water uptake model:

$$\beta(r, z) = \left(1 - \frac{z}{Z_m} \right) \left(1 - \frac{r}{R_m} \right) e^{-[(p_z/Z_m)|z^* - z| + (p_r/R_m)|r^* - r|]}, \quad (3)$$

where R_m (L) is the maximum rooting length in the radial direction, r (L) is the radial distance from the origin of the tree, and p_r (dimensionless) and r^* (L) are additional empirical parameters. Here $\beta(r, z)$ (dimensionless) denotes the two-dimensional spatial distribution of potential root water uptake. *Vrugt et al.* [2001b] showed that the root water uptake in (3) is extremely flexible and allows spatial variations of water

uptake as influenced by nonuniform water application (e.g., drip irrigation) and root length density patterns.

Including an additional exponential term in (3) leads to a three-dimensional root water uptake model, which is expressed as

$$\beta(x, y, z) = \left(1 - \frac{x}{X_m}\right)\left(1 - \frac{y}{Y_m}\right)$$

$$\cdot \left(1 - \frac{z}{Z_m}\right) e^{-[(p_x/X_m)|x^*-x| + (p_y/Y_m)|y^*-y| + (p_z/Z_m)|z^*-z|]}, \quad (4)$$

where X_m and Y_m (L) are the maximum rooting length in the x and y direction; x and y (L) are the distances from the origin of the tree in the x and y direction; p_x (dimensionless), p_y (dimensionless), x^* (L), and y^* (L) are empirical parameters; and $\beta(x, y, z)$ (dimensionless) denotes the three-dimensional spatial distribution of potential root water uptake. As in (1) we set p_x, p_y, and p_z to unity for $z > z^*$, $x > x^*$ and $y > y^*$, respectively.

Denoting the normalized root water uptake S_m $(L^3 \ L^{-3} \ T^{-1})$ as the volume of water extracted per unit volume of soil with time, it follows that
One-dimensional description

$$S_m(z) = \frac{\beta(z)T_{pot}}{\int_0^{Z_m} \beta(z) \ dz}, \quad (5a)$$

Two-dimensional axial symmetry

$$S_m(r, z) = \frac{\pi R^2 \beta(r, z)T_{pot}}{2\pi \int_0^{Z_m} \int_0^{R_m} r\beta(r, z) \ dr \ dz}, \quad (5b)$$

Three-dimensional description

$$S_m(x, y, z) = \frac{X_m Y_m \beta(x, y, z)T_{pot}}{\int_0^{X_m} \int_0^{Y_m} \int_0^{Z_m} \beta(x, y, z) \ dx \ dy \ dz}. \quad (5c)$$

So integration of any of the above expressions over the spatial domain leads to the result that cumulative potential root water uptake is equal to the potential transpiration T_{pot}.

To provide for root water uptake under water-stressed conditions, a soil water stress response function was included [*Van Genuchten*, 1987],

$$\gamma(h) = \frac{1}{\left[1 + \left(\frac{h(x, y, z, t)}{h_{50}}\right)^p\right]}, \quad (6)$$

where h is the soil water matric head at a particular spatial location, h_{50} (L) is the soil water pressure head at which root water uptake rate is reduced by 50%, and p (dimensionless) is a fitting parameter. The parameter p is usually assumed to be 3 [*Van Genuchten and Gupta*, 1993].

Finally, the actual root water uptake rate at any particular spatial location can be calculated from

$$S(h, x, y, z) = \gamma(h)S_m(x, y, z), \quad (7)$$

where for an almond tree,

$$T_{pot} = ET_{almond} - E_s \quad (8)$$

where $S(h, x, y, z)$ (T^{-1}) is the actual root water uptake and E_s $(L \ T^{-1})$ denotes soil evaporation. ET_{almond} defines the potential ET by the almond crop and is computed from the product of K_c and ET_0, where K_c is the crop coefficient (dimensionless), and ET_0 $(L \ T^{-1})$ is the reference evapotranspiration. Hence the actual transpiration rate T_a can be computed from
One-dimensional (1-D)

$$T_a = \int_0^{Z_m} S(h, z) \ dz, \quad (9a)$$

Axial symmetrical (2-D)

$$T_a = \frac{2\pi}{\pi R^2} \int_0^{Z_m} \int_0^{R_m} rS(h, r, z) \ dr \ dz, \quad (9b)$$

Three-dimensional (3-D)

$$T_a = \frac{1}{X_m Y_m} \int_0^{X_m} \int_0^{Y_m} \int_0^{Z_m} S(h, x, y, z) \ dx \ dy \ dz. \quad (9c)$$

2.2. Field Description and Measurements

The experimental plot of our almond orchard includes about one quarter of the wetted area of a microsprinkler irrigating a single almond tree [*Koumanov et al.*, 1997; *Vrugt et al.*, 2001b]. Hence, despite the spatial variability in irrigation amounts by the microsprinkler, we assumed that this instrumented area of 2.0×2.0 m (Figure 1) was representative. Twenty-five PVC neutron probe access tubes were installed in a square grid of 0.50-m spacing to a depth of 90 cm. The neutron probe was calibrated from gravimetric measurements using soil samples collected at soil depths of 15, 30, 45, 60, 75, and 90 cm during and after access tube installation. Separate calibration curves were used for the 0–15 cm surface soil and the 30–90 cm soil depth interval. Standard errors of the estimate of volumetric water content curves were ~0.01 m^3 m^{-3} at the 15 cm depth interval and 0.02 m^3 m^{-3} at all other measurements depths. The field is slightly undulating, and the soil is a shallow gravelly loam [*Andreu et al.*, 1997], overlaying a sloping high-density restricting clay layer at about the 90–120 cm soil depth. The studies by *Andreu et al.* [1997] and *Koumanov et al.* [1997] indicated that root water uptake during the growing season was mainly limited to the top 40–60 cm and that drainage at the 90 cm depth occurred primarily by lateral flow along the sloping restricting clay layer.

The measurements were conducted during the September 13–29 period in the summer of 1995, after the microsprinkler system was used to wet up the whole soil profile. Neutron probe measurements were taken on September 13, immediately after the irrigation at 1300, 1500, and 1800 LT; during the period September 14 through September 17, every 4 hours at 600, 1000, 1400, and 1800 LT; and during the period September 18 through September 29, daily at ~1000 LT. This resulted in 31 water content measurements at each spatial location. To test the one- and two-dimensional root water uptake model, the three-dimensional local measurements of water content were reduced to one and two dimensions, respectively. For one dimension, all the water content measurements at a specific depth for all x and y locations were arithmetically averaged.
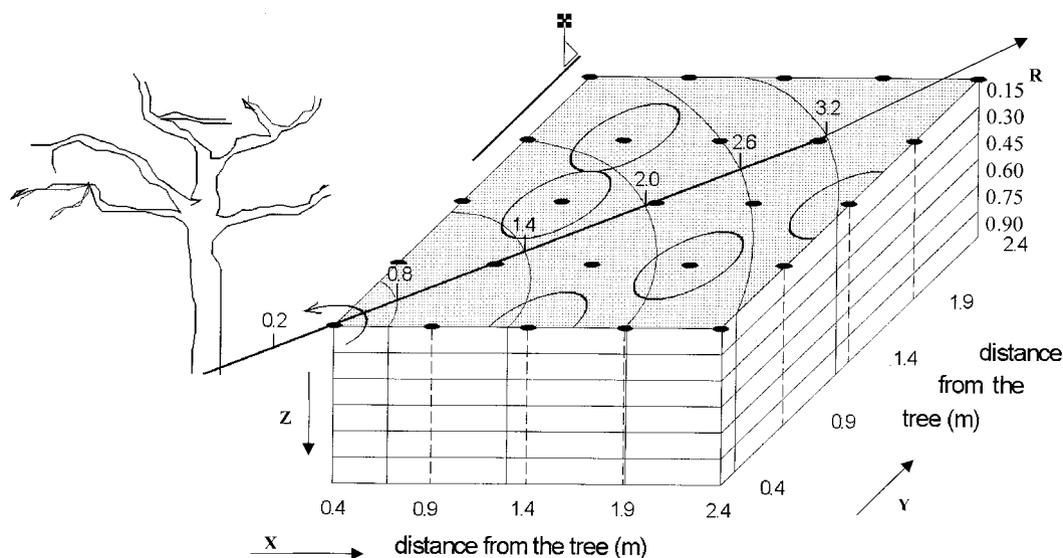
Figure 1. Schematic view of the experimental plot. Location of the neutron probe access tubes is indicated by solid dots. Circles approximate neutron probe measurement volumes, and curved lines indicate the averaging volumes for the two-dimensional simulations.

Hence the one-dimensional data set was determined from 31 water content values at each depth and measurement time during the September 13–29 monitoring period.

To simplify testing of the two-dimensional root water uptake model, the three-dimensional grid measurements of water content needed to be reduced to two dimensions (r and z). For this we assumed that (1) the root water uptake around the tree was axisymmetrical and (2) the measurement volume of the neutron probe water content measurements was a sphere with a constant radius of ~0.25 m.

For each depth interval the rectangular measurement grid of Figure 1 was partitioned into five concentric 0.6 m wide circular strips with their origin determined by the neutron access pipe location closest to the tree trunk. Second, a radial average water content value was computed for each of the five soil areas (0.2–0.8, 0.8–1.4, 1.4–2.0, 2.0–2.6, and 2.6–3.2 m concentric circles) using weighting factors for each neutron probe location with values equal to the fraction of the measurement volume fitting within the respective concentric soil area. We used 0.6 m wide strips for each of the five soil areas to ensure that enough water content measurements were contained within the respective strip. Moreover, the averaging using the 0.6 m wide strips gave the best agreement in total water depletion of the reduced two-dimensional domain as compared to the original three-dimensional grid of water content measurements. Since the averaging procedure was applied to depth intervals of 0–0.15, 0.15–0.3, 0.3–0.45, and 0.45–0.6 m during the September 13–29 period, the final two-dimensional map included 20 average water content values at each measurement time, namely, four depth intervals and five radial distance increments.

In Figure 2 we present the measured three-dimensional volumetric water content distributions at three different times during the monitoring period, as illustrated by depth interval–averaged water content values. At the beginning of the period, volumetric water content values are ~0.24 m³ m⁻³ at the soil surface and increase downward to ~0.28 m³ m⁻³. Clearly, as time proceeds, the water content at the 60 cm depth is still

relatively high, whereas a water uptake pattern is becoming apparent in the surface layers, with volumetric water content values ranging between 0.04 and 0.08 m³ m⁻³ in the top soil layers.

2.3. Soil Water Flow Modeling

The adapted models that solved for the one-, two-, and three-dimensional solutions of (1) were HYDRUS-1D [*Šimunek et al.*, 1998], HYDRUS-2D [*Šimunek et al.*, 1999], and HYDRUS-3D (update of the SWMS_3D code of *Šimunek et al.* [1995]), respectively. All three models use the Galerkin finite element method based on the mass conservative iterative scheme proposed by *Celia et al.* [1990].

The unsaturated hydraulic properties for all three models are defined by [*Van Genuchten*, 1980; *Mualem*, 1976]

$$S_e = \frac{\theta(h) - \theta_r}{\theta_s - \theta_r} = [1 + (\alpha|h|)^n]^{-m} \qquad m = \frac{n - 1}{n} \qquad (10)$$

$$K(\theta) = K_s S_e^{0.5}[1 - (1 - S_e^{1/m})^m]^2, \qquad (11)$$

where θ_s ($L^3 L^{-3}$) is the saturated water content, ($L^3 L^{-3}$) is the residual water content, α (L^{-1}) and n (dimensionless) are curve shape parameters, and K_s ($L T^{-1}$) denotes the saturated hydraulic conductivity.

In the preprocessing phase the soil domain was discretized into a rectangular grid of finite elements with similar size elements defining the spatial resolution to avoid differences in truncation errors between the three simulation models. For all three simulation models the vertical domain was 0.6 m deep. In HYDRUS-1D the vertical domain was discretized into 40 equidistant finite elements. For the two-dimensional model the simulated flow domain was 3 m long in the radial direction, using a grid spacing of 0.05 m in the radial and 0.015 m in the vertical direction. For the three-dimensional simulations the dimension of the soil domain was 0.15 by 2.65 m in the *x*-*y* plane. The flow domain was discretized into a structured mesh of 13,500 blocks corresponding with 14,400 nodes, with a variable node spacing between 0.01 and 0.10 m. A structured mesh
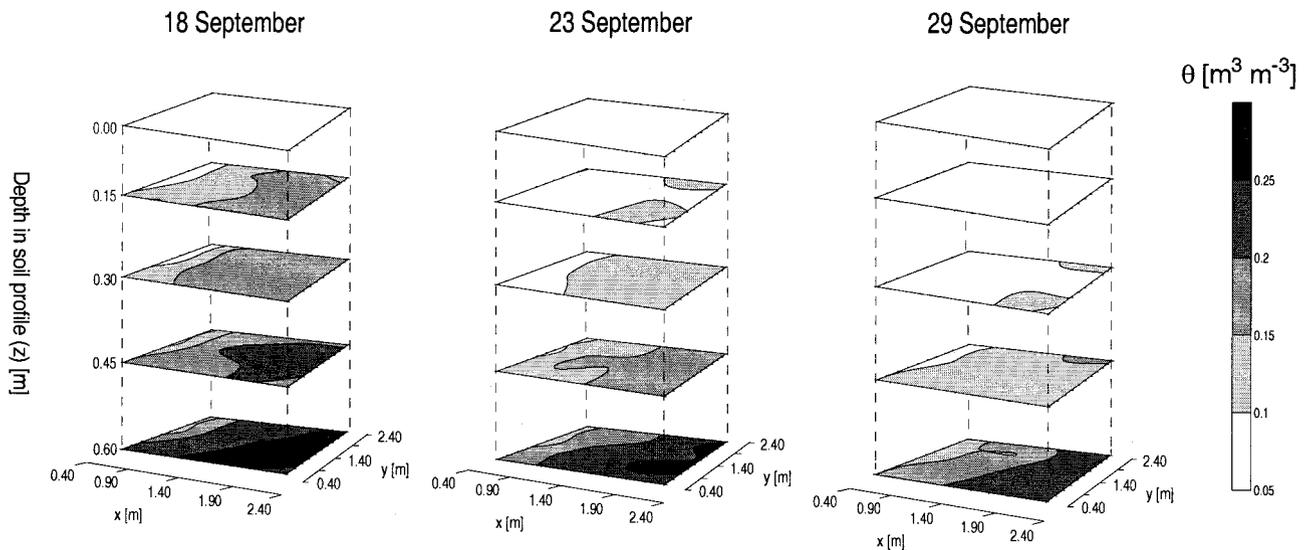
Figure 2. Measured three-dimensional volumetric water content distributions at three different times during the monitoring period.

was used to avoid large errors between measured and computed water content values at nodes with overlapping neutron probe measurement volumes and was a compromise between available computing time and nodal density.

Figure 3 presents the daily estimated boundary conditions as function of time during the monitoring period. Numerical modeling requires estimates of potential transpiration T_{pot} and soil evaporation E_s. As no direct measurement of the transpiration of the almond tree was available, we used the following approach. Daily reference evapotranspiration ET_0 were provided by a nearby weather station of the California Irrigation Management Information System (CIMIS). Almond potential ET_{almond} was calculated from ET_0 and the appropriate crop coefficients K_c. *Snyder and Pruitt* [1988] recommended a value for K_c of 0.91, corresponding to conditions of 60% canopy soil surface coverage for drip-irrigated trees in the Sacramento Valley. *Ritchie*'s [1972] equation was used to estimate soil evaporation. The radiation interception was calculated using the empirical function for maize [*Snyder et al.*, 1985], while we used an upper limit of stage 1 cumulative soil water evapora-

tion of 6 mm and a partitioning factor of 0.4 between stage 1 and stage 2 evaporation [*Ritchie*, 1972]. The potential transpiration of almond trees T_{pot} was obtained by subtracting the soil evaporation from ET_{almond} (equation (7b)). Although we agree that this approach for calculating T_{pot} is quite simplistic, it is to be expected that errors in estimated daily T_{pot} amounts are smaller than 10%. We should also note that the focus of this study was to demonstrate the development and functionality of spatially distributed root water uptake models.

Owing to the lack of accurate flux information, we assumed a unit hydraulic gradient at the lower boundary (gravity flow). This approach seemed most appropriate since water balance calculations using the estimated ET and measured infiltration data indicated that a drainage term was required to match measured soil water storage data changes. The water content measurements immediately after the irrigation of September 13 were used as initial condition for all numerical simulations.

2.4. Parameter Optimization by Inverse Modeling

In the inverse modeling stage of this study a total of 6 (e.g., Z_m, p_z, z^*, n, K_s, and h_{50}), 9 (e.g., Z_m, p_z, z^*, R_m, p_r, r^*, n, K_s, and h_{50}), and 12 (e.g., X_m, p_x, x^*, Y_m, p_y, y^*, Z_m, p_z, z^*, n, K_s, and h_{50}) root water uptake and soil hydraulic parameters were identified simultaneously using the one-, two-, and three-dimensional HYDRUS models, respectively. Despite measurement of the soil hydraulic properties of a nearby location in the same almond orchard [*Andreu et al.*, 1997], the soil heterogeneity within the orchard led us to also optimize some of the soil hydraulic parameters simultaneously with the respective root water uptake model parameters. While fixing the parameters θ_s and α to reported values [*Andreu et al.*, 1997] of 0.30 m^3 m^{-3} and 9.4 m^{-1}, respectively, the soil hydraulic properties were assumed to be characterized by the fitting parameters n and K_s of (10) and (11). Since some of the measured water content values were smaller than the residual water content values reported by *Andreu et al.* [1997], the residual water content θ_r was fixed to 0.0 m^3 m^{-3}.
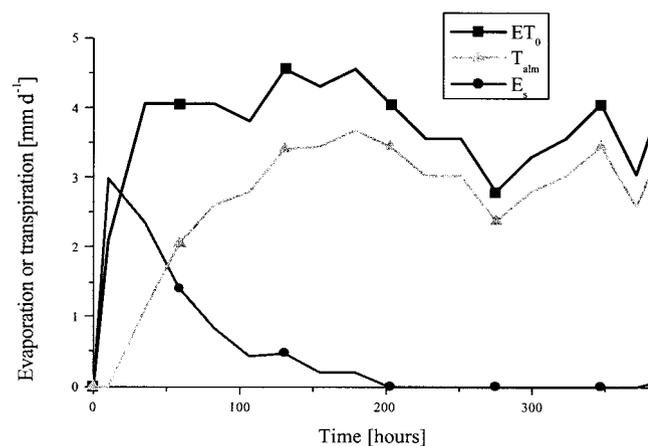
Since optimization algorithms such as Levenberg-Marquardt or Simplex method are generally only applicable to identify a limited number of unique parameters, an alternative was

Figure 3. Soil surface boundary conditions during simulation period (Time 0 corresponds with September 13).

Table 1. Range of Parameter Values Used With Genetic Algorithm (GA) With HYDRUS-1D, HYDRUS-2D, and HYDRUS-3D Simulations

	HYDRUS-1D					
	Z_m, m	z^*, m	p_z	h_{50}, m	n	K_s, cm d^{-1}
Minimum	0.00	1.00	0.10	-0.20	1.20	1×10^{-2}
Maximum	1.00	5.00	15.0	-10.0	3.00	100.00

	HYDRUS-2D							
	Z_m, m	R_m, m	x^*, m	r^*, m	p_z	p_r	h_{50}, m	n	K_s, cm d^{-1}
Minimum	0.00	1.00	0.00	1.00	0.10	0.10	-0.20	1.20	1×10^{-2}
Maximum	1.00	5.00	1.00	5.00	15.0	15.0	-10.0	3.00	100.00

	HYDRUS-3D											
	X_m, m	Y_m, m	Z_m, m	x^*, m	y^*, m	z^*, m	p_x	p_y	p_z	h_{50}, m	n	K_s, cm d^{-1}
Minimum	1.00	1.00	0.00	1.00	1.00	0.00	0.10	0.10	0.10	-0.20	1.20	1×10^{-2}
Maximum	5.00	5.00	1.00	5.00	5.00	1.00	15.0	15.0	15.0	-10.0	3.00	100.00

needed to optimize the larger set of parameters of this study. Recently, it has been shown that genetic algorithms (GA) are a powerful tool for parameter identification, if the number of fitted parameters is large [*Bäck*, 1996; *Wang*, 1991; *Holland*, 1975]. The genetic algorithm is a search procedure based on the mechanics of natural selection and natural genetics that combines an artificial survival of the fittest with genetic operators [*Holland*, 1975]. The GA differs from other search methods as it searches among a population of parameter sets rather than the parameter values themselves using probabilistic transition rules. We applied the GA presented by *Penny and Lindfield* [1995] with the small adaptation that the best performing parameter combination is not mutated in the next generation. We used a crossover percentage of 85 to ensure a relatively fast convergence to the global optimum, whereas a mutation factor of 0.15 was used to avoid optimized solutions in local minima. The population size, representing the number of first generation parameter combinations, was set to 120, whereas the final optimized parameter combination was selected after 200 generations. Assuming that the residuals, representing errors between measured and optimized volumetric water content values, are Gaussian distributed, independent, and homocedastic (constant variance), the fitness of a chromosome was calculated by the following objective function (OF):

$$OF(\mathbf{b}) = \sum_{i=1}^{N} [\theta^*(t_i) - \theta(t_i, \mathbf{b})]^2, \quad (12)$$

where N is the number of observations and $\theta^*(t_i)$ and $\theta(t_i, \mathbf{b})$ denote the measured and predicted water content values, respectively, at time t_i. The parameter vector $\mathbf{b}$ characterizes the chromosome with the genes representing the fitting parameters. The allowable ranges of the parameters included in $\mathbf{b}$ for each numerical model are presented in Table 1.

Although GAs are an effective means of reaching the global minimum region, they are not necessarily efficient in finding the exact optimum location. Therefore the results of the genetic algorithm were used as initial values for a subsequent Simplex algorithm (SA) to determine the local minimum of OF within the global minimum region as determined by the GA. Using a sensitivity analysis in which each parameter was varied

with 10% of its final optimized value, while keeping the additional parameters fixed at their value determined by the GA, only those six parameters that were most sensitive to model output were fine-tuned. Both the GA and Simplex optimization were carried out using MATLAB, version 5.3 [*The MathWorks*, 1999].

The uncertainty of each optimized parameter $\mathbf{b}_j, j = 1, \ldots, m$, was determined from the diagonal elements of the parameter covariance matrix $\mathbf{C}$ [*Kool and Parker*, 1988; *Šimunek and Hopmans*, 2001], representing the estimate of the standard deviation s_j,

$$s_j = \sqrt{\mathbf{C}_{jj}}, \quad (13)$$

whereas model performance was evaluated by the root mean squared error (RMSE), computed from

$$\mathrm{RMSE} = \sqrt{\frac{\sum_{i=1}^{N} [\theta^*(t_i) - \theta(t_i, \mathbf{b})]^2}{N - m}}, \quad (14)$$

where N and m denote the number of measurements and total number of parameters, respectively.

A single forward simulation of the HYDRUS-3D model required between 5 and 60 min on a PIII 466 MHz computer, depending on the parameter combination provided. So the computational time for one computer to perform all 24,000 model runs for the GA optimization iterations was extremely long. Instead, we used 40 PIII 400 MHz slave computers connected with one master computer to perform the optimizations.

3. Results and Discussion

3.1. Three-Dimensional Simulations

The parameter vector of the best performing "chromosome" of the final population after 200 generations of the three-dimensional root water uptake parameters using GA in combination with the HYDRUS-3D flow model is presented in Table 2. Also included are the final results after final tuning of the selected parameters using the SA with their confidence

Table 2. Optimized Parameter Values and Their 95% Confidence Intervals After Genetic Algorithms (GA) and Simplex Algorithm (SA) for the HYDRUS-3D Model[a]

| | HYDRUS-3D | | 95% Confidence Interval | | |
Parameter	GA	SA	Lower	Upper	CV[b]
		Root Model			
X_m, m	3.31		2.84	3.77	7.10
Y_m, m	2.65	2.60	2.43	2.78	3.46
Z_m, m	0.43	0.45	0.32	0.57	13.33
p_x	1.86		1.67	2.06	5.38
p_y	2.62		2.46	2.77	2.86
p_z	2.57		2.24	2.89	6.23
x^*, m	1.92		1.61	2.22	7.81
y^*, m	1.92	2.21	1.64	2.42	4.75
z^*, m	0.35	0.40	−0.06	0.86	57.50
		Soil Hydraulic Model			
n	1.72	1.74	1.71	1.78	1.15
K_s, cm d^{-1}	1.82	1.60	0.10	3.10	46.88
h_{50}, m	−0.85		−1.05	−0.64	12.35
RMSE, m^3 m^{-3}	0.0183	0.0180			
R^2	0.91	0.92			
		Derived Parameters			
X_0, m	1.53	1.53			
Y_0, m	1.64	1.61			
Z_0, m	0.26	0.27			

[a]Open space means parameter held constant to value found by genetic algorithm.
[b]CV is coefficient of variation.

intervals, values for the derived parameters X_0, Y_0, and Z_0, and RMSE and R^2 values. The optimum maximum rooting depth Z_m ($0.43 < Z_m < 0.45$ m) is in excellent agreement with the results obtained by *Koumanov et al.* [1997] for the same experimental plot, confirming that active root water uptake was limited to the top 40 cm only. The position of maximum root water uptake of the almond tree under nonstressed conditions ($X_0 = 1.53$, $Y_0 = 1.61$, $Z_0 = 0.27$ m) agrees well with the surface area of maximum irrigation application by microsprinkling [*Koumanov et al.*, 1997]. This was so despite the location of the microsprinkler at the far corner along the tree row (see Figure 1), as caused by nonuniform water applications during the growing season. The optimized n value of the soil hydraulic functions ($n = 1.74$) agrees well with the reported n value ($n = 1.44 − 1.99$) for this soil obtained with the instantaneous profile method [*Andreu et al.*, 1997]. The relatively high value of the h_{50} parameter ($h_{50} = −0.85$ m) is an indication of the small water holding capacity of this coarse-textured soil. The optimized saturated conductivity ($K_s = 1.60$ cm d^{-1}) is lower than the reported range of 34.1–62.4 cm d^{-1} measured under saturated conditions for the 0–60 cm depth interval [*Andreu et al.*, 1997]. The lower optimized K_s value is to be expected since the measured experimental conditions were such that the soil rooting zone was less than saturated, thereby eliminating the influence of the macropores on the estimated K_s. Using the same data set for their two-dimensional analysis, *Vrugt et al.* [2001b] showed that the HYDRUS-2D model was well able to predict water content dynamics for spatial locations not included in the calibration period.

The measured water content values for all depths and measurement locations are correlated with simulated water content values using the final optimized parameter values in Figure 4. Measured values match the simulated values with an R^2 value of 0.92. The overall RMSE value of 0.018 m^3 m^{-3} is low,

considering that the standard errors of the neutron probe water content measurements are already 0.01 m^3 m^{-3} (15 cm depth) and 0.02 m^3 m^{-3} (all other soil depths).

Figure 5 presents three-dimensional maps of simulated water content and root water uptake intensity, $S_m(x, y, z)$, averaged for the indicated soil compartments (0–0.15, 0.15–0.30, 0.30–0.45, and 0.45–0.60 m) at the three different times of September 18, 23, and 29. These maps were obtained from arithmetic averaging over all nodal values within each depth interval followed by interpolation using SURFER [*Golden Software*, 1996]. At the beginning of the period, after irrigation on September 13, maximum actual water uptake rates approached 8×10^{-4} m^3 m^{-3} hr^{-1}. As the soil becomes depleted

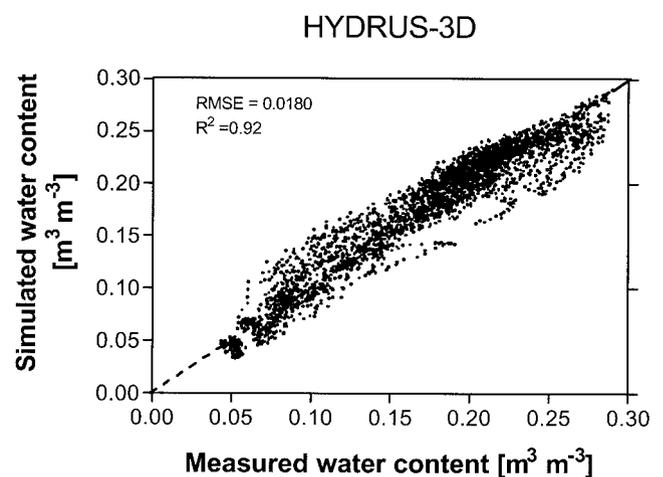**HYDRUS-3D**

RMSE = 0.0180
R^2 = 0.92

Figure 4. Measured versus simulated soil water contents around the almond tree obtained using the calibrated HYDRUS-3D model.
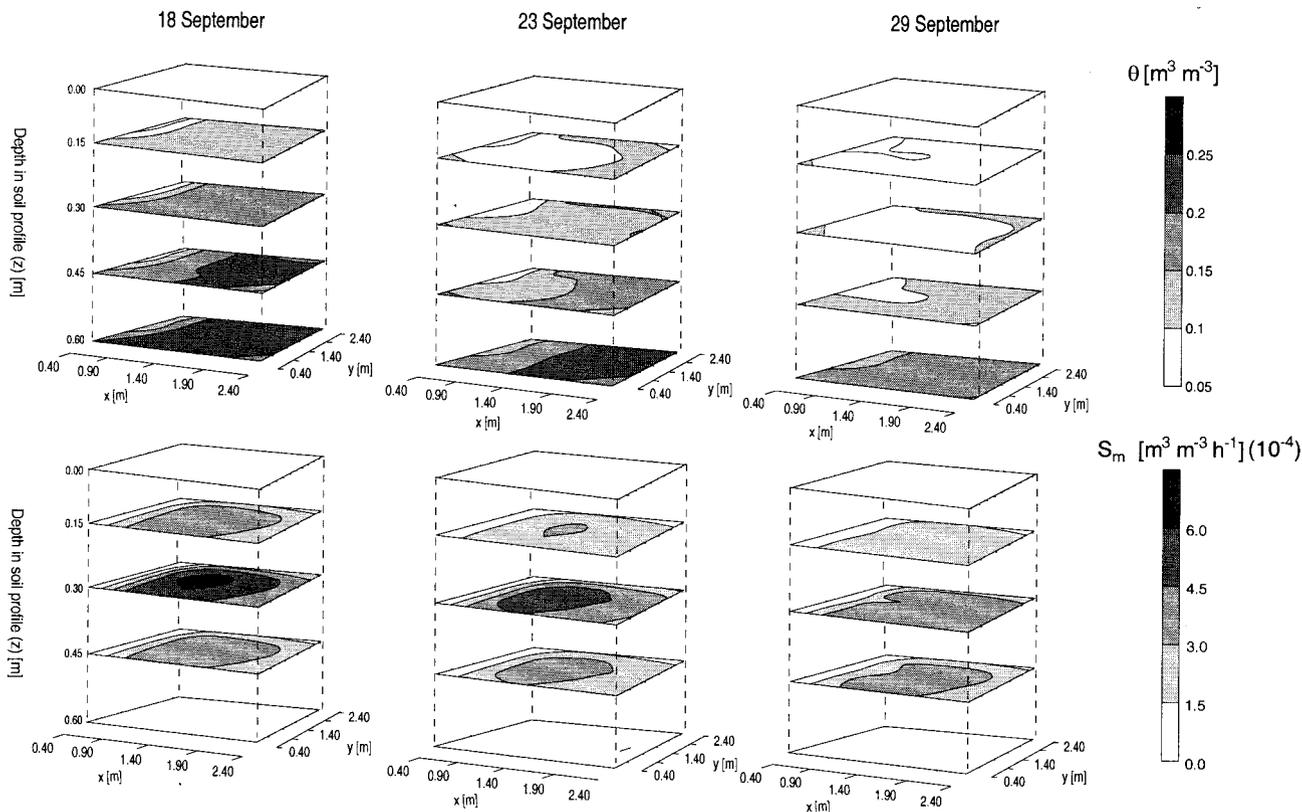
Figure 5. Simulated three-dimensional volumetric water content and potential root water uptake distributions at three times during the monitoring period.

in water, regions of maximum root water uptake shifted to other locations within the rooting zone where soil water was most readily available [*Green and Clothier*, 1999]. For example, close observation of Figure 5 shows that the general root water uptake pattern changes with time from maximum uptake around (X_0, Y_0, Z_0) toward the outside perimeter of the rooting volume, as caused by changes in soil water stress with time. Although there are differences in the spatial pattern of soil water content between simulated and measured water content values (compare Figures 2 and 5), the magnitude of simulated water contents at the different depth intervals agreed well with the measured water contents.

In Figure 6a we present contour plots of the time-averaged RMSE of water content at the four depth intervals. These contour plots were computed using arithmetic averaging of all nodal values within the respective soil volume of the corresponding neutron probe measurement and thus resulted in 25 RMSE values for each depth interval. Although, in general, RMSE values are small, relatively large error values are present at the bottom corner in the spatial domain near $x = 2.4$ m and $y = 0.4$ m. Differences between measured and simulated water content values are likely because of model errors as caused by restrictive assumptions regarding the geometry of the rooting system, homogeneity of soil hydraulic properties within the spatial domain, and the prescribed root water uptake model. For example, the water uptake model assumes a single region of maximum uptake, whereas in reality more regions within the rooting zone may show local maximum uptake as caused by water application nonuniformities and soil environmental factors affecting root growth. Figure 6b presents a box plot of the time averaged RMSE values for all 100

spatial locations (25 tubes $\times$ 4 depth intervals). The box plot shows the single outlier with RMSE = 0.04 at $1.9 < x < 2.4$ m in the bottom right-hand corner of the spatial domain as well as a clear clustering of RMSE values between 0.01 and 0.02 m^3 m^{-3}, with their magnitude about equal to the standard error of the water content measurements with the neutron probe. The various horizontal lines represent the minimum, maximum, 25th percentile, mean, and 75th percentile of the RMSE values, respectively.

3.2. Dimensional Effects on Parameter Optimization Results

Final optimized parameter values after using the GA and fine-tuning with the SA for the HYDRUS-1D, HYDRUS-2D, and HYDRUS-3D models and their 95% confidence intervals are presented in Table 3. Also included are the derived parameter values of X_0, Y_0, and Z_0 and the fitting results as expressed by the RMSE and R^2 values. Since many errors may occur, including measurement, model, and numerical errors, an uncertainty analysis of the optimized parameters makes up an important part of parameter estimation. Therefore we included 95% confidence intervals for the optimized parameters, calculated using the Jacobian matrices and residuals for the final optimized solution.

As Table 3 shows, optimized parameter values for the maximum rooting depth Z_m (0.41–0.49 m), n (1.74–1.91), h_{50} (-0.53 to -0.85 m), and Z_0 (0.27–0.28 m) are close between the three cases. It indicates that the information content of the water content measurements, whether aggregated or not, is the most robust for these parameters [*Vrugt et al.*, 2001a]. To obtain convergence of the inverse solution it was essential to
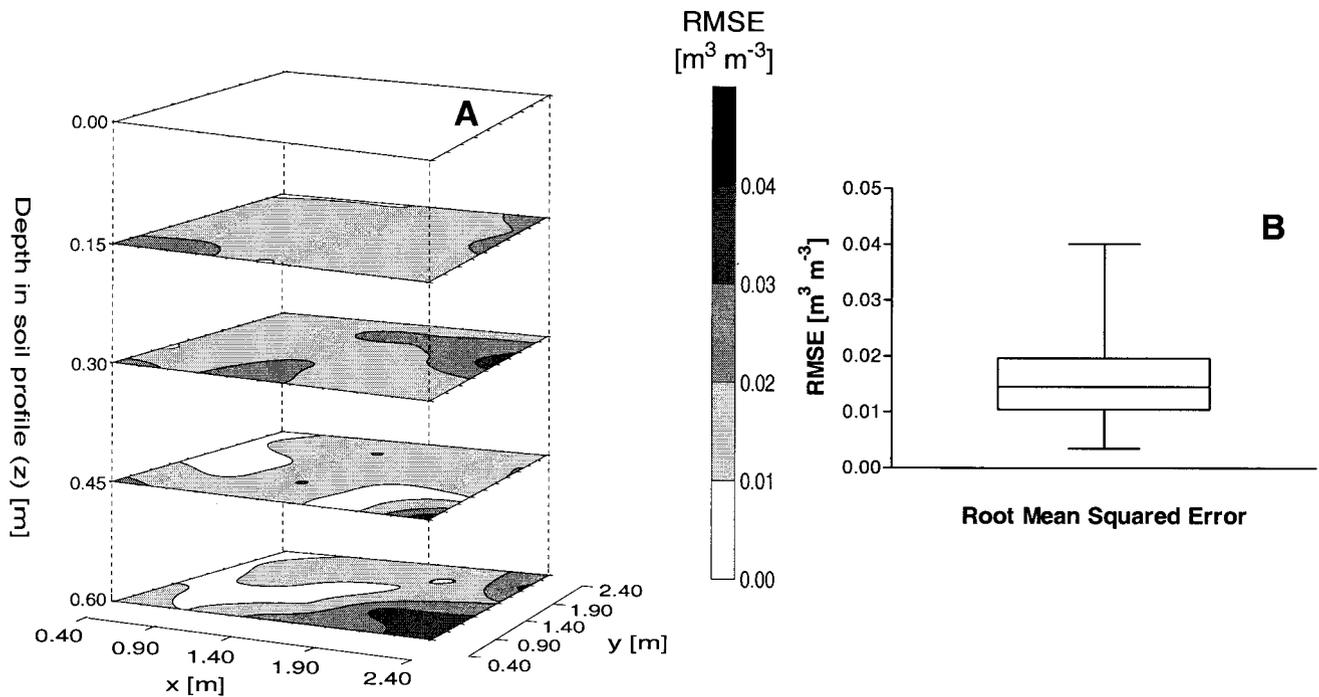
Figure 6. (a) Three-dimensional spatial distribution of root mean squared errors of water content. (b) Box plot of RMSE for all measured locations and times.

select initial values for the other parameters, close to their expected values [*Inoue et al.*, 1998]. Problems with nonuniqueness of these parameters are caused by the presence of numerous local minima, as can occur when this many parameters are

optimized simultaneously [*Duan et al.*, 1992]. Whereas all our optimization results for the numerical models indicate the depth of maximum root water uptake to be at ~0.25 m, the study by *Andreu et al.* [1997] concluded that maximum uptake

Table 3. Optimized Parameter Values and Their 95% Confidence Regions After Simplex Algorithm (SA) for the HYDRUS-1D and HYDRUS-2D Models[a]

Parameter	HYDRUS-1D Optimized Value (Confidence Interval)	CV	HYDRUS-2D Optimized Value (Confidence Interval)	CV	HYDRUS-3D Optimized Value (Confidence Interval)	CV
			Root Model			
X_m, m					3.31 ± 0.46	7.10
Y_m, m					2.60 ± 0.18	3.46
Z_m, m	0.49 ± 0.045	4.21	0.41 ± 0.49	10.76	0.45 ± 0.13	13.33
R_m, m			3.99 ± 0.49	6.22		
p_x					1.86 ± 0.20	5.38
p_y					2.62 ± 0.15	2.86
p_z	2.98 ± 0.74	12.49	3.32 ± 4.14	12.64	2.57 ± 0.32	6.23
p_r			3.44 ± 0.55	8.18		
x^*, m					1.92 ± 0.30	7.81
y^*, m					2.21 ± 0.21	4.75
z^*, m	0.27 ± 0.04	7.09	0.31 ± 0.13	20.79	0.40 ± 0.46	57.50
r^*, m			1.96 ± 0.18	4.53		
			Soil Hydraulic Model			
n	1.91 ± 0.22	13.56	1.75 ± 0.11	3.26	1.74 ± 0.04	1.15
K_s, cm d^{-1}	0.72 ± 0.19	8.76	0.75 ± 0.16	10.93	1.60 ± 1.50	46.88
h_{50}, m	-0.76 ± -0.13	5.89	-0.53 ± -0.16	15.10	-0.85 ± -0.21	12.35
RMSE, m^3 m^{-3}	0.0068		0.0154		0.0180	
R^2	0.98		0.91		0.92	
			Derived Parameters			
X_0, m					1.53	
Y_0, m					1.61	
Z_0, m	0.27		0.28		0.27	
R_0, m			1.96			

[a]For completeness we also report the HYDRUS-3D model results.
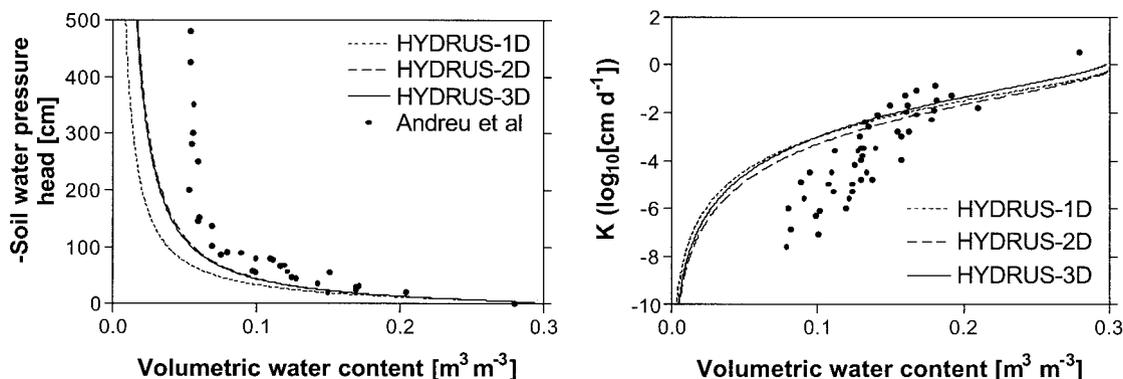
Figure 7. Optimized soil water retention curves using HYDRUS-1D, HYDRUS-2D, and HYDRUS-3D flow models with corresponding multidimensional root water uptake models. Also included are independently measured (θ, h) points [*Andreu et al.*, 1997].

occurred at the soil surface (0–15 cm) and decreased further down the soil profile. However, their study did not include soil evaporation as a possible mechanism of soil water depletion near the soil surface. The coefficient of variation (CV) indicates that for most parameters the confidence intervals at the minimum are typically small (CV < 10%).

The optimized soil water retention and unsaturated soil hydraulic functions of the HYDRUS-1D, HYDRUS-2D, and HYDRUS-3D models are presented in Figure 7. Also included are the measured (θ, h) data using the multistep outflow method from soil cores taken at the 30 cm soil depth for a nearby location. Both the measured (θ, h) points and the optimized retention curves clearly show the small water holding capacity of this shallow gravely soil. Whereas the optimized retention functions of the HYDRUS-2D and HYDRUS-3D model match extremely well, the HYDRUS-1D optimization shifts the water retention to an even more coarser-textured soil, increasing drainage as compared to the multidimensional flow models. Differences between independently measured (θ, h) points and the optimized curves mostly occur outside the range of experimental water content values $(\theta < 0.08)$ and are most likely caused by the sensitivity of the optimized retention curve to the fixed residual water content value $(\theta_r = 0)$. Clearly, parameters obtained with parameter estimation are to be used only within the measurement range for which they were determined [*Inoue et al.*, 2000; *Vrugt et al.*, 2001a]. Additionally, the optimized unsaturated hydraulic conductivity and measured (K, θ) points show the rapid decrease of the hydraulic conductivity with decreasing water content. The optimized saturated conductivity of 0.46 cm d^{-1} of the SA optimization is much lower than the reported range of 34.1–62.4 cm d^{-1} measured under saturated conditions for the 0–60 cm depth interval by *Andreu et al.* [1997]. However, one should realize that the saturated hydraulic conductivity in this study is much more a water balance parameter, controlling the magnitude of the lower boundary flux, than it is a soil physical parameter affecting soil water flow in the soil domain. Moreover, the saturated conductivity determined by *Andreu et al.* [1997] was measured under saturated conditions, when macropores play a major role.

Although not presented, the parameter correlation matrix for the one-, two-, and three-dimensional models using the off-diagonal terms of the covariance matrix showed that correlations were typically low for the three-dimensional (3-D)

optimizations but that parameter correlations increased when decreasing spatial dimensions (2-D and 1-D). For example, the correlation between the parameters n and h_{50} was high ($R = 0.99$) for the 2-D model. Low parameter correlations are important as they increase the likelihood of uniqueness of the final solution. The decrease in parameter correlation with increasing flow dimensions is likely caused by the corresponding increase in number of observations used in the optimization, relative to the increasing number of fitting parameters. As shown in Figure 8, the simulated water contents with the final parameter estimates obtained with the SA compare favorably with the corresponding measured water contents for both the HYDRUS-1D and the HYDRUS-2D model. The increase in RMSE with increasing model dimension is caused by the significantly increased number of water content observations (3-D versus 2-D and 1-D) included in the objective function (equation (12)) with increasing spatial dimension of the optimization problem. This is especially the case as the number of fitting parameters increased only slightly with spatial dimension. Moreover, the averaging of the water contents used in the one- and two-dimensional simulations reduced the general water content variability, thereby decreasing the final RMSE values.

Figure 9 presents a comparison between the optimized spatial distributions of potential root water uptake over the spatial domain as obtained using the one-, two-, and three-dimensional root water uptake and flow models. Starting with the three-dimensional model results, spatial values of the optimized potential root water uptake function, $\beta(x, y, z)$, were arithmetically averaged and subsequently normalized in the radial direction (equation (5b)) to obtain an average $S_m(r, z)$. Subsequently, a similar averaging procedure was carried out in the radial direction to show the average $S_m(z)$. Using the two-dimensional flow and root uptake model, spatially averaging and normalization (equation (5a)) of $S_m(r, z)$ resulted in another average $S_m(z)$. The close match between the three one-dimensional potential root water uptake distributions in Figure 10 indicates that the suggested aggregation of measured three-dimensional water content measurements to arrive at two- and one-dimensional root water uptake models is valid.

In Table 4 we present the different water balance components with their spatial variations (standard deviations) as simulated by the HYDRUS-1D, HYDRUS-2D, and HYDRUS-3D models. Spatial variability in drainage flux was computed from simulated flux density values at the 55 cm soil
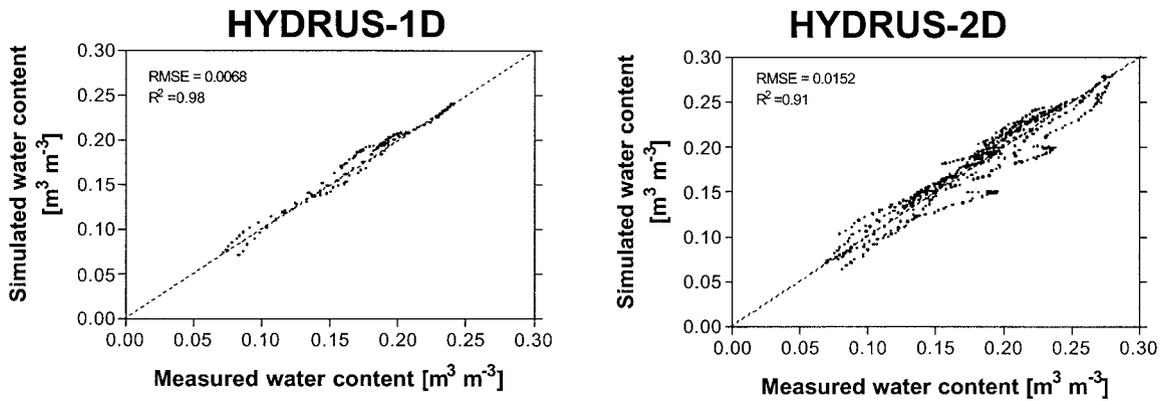
Figure 8. Measured versus simulated soil water contents around the almond tree after parameter optimization using HYDRUS-1D and HYDRUS-2D flow models.

depth. The agreement between the various listed water balance components for the different numerical models is satisfactory. As different numerical models are used with differences in aggregation of water content values between spatial dimensions, perfect agreement is unlikely. Cumulative soil evaporation and drainage components are typically small compared to total cumulative root water uptake. Differences between actual and potential transpiration are caused by water stress (differences between T_{pot} and T_a). As soil water storage is used in the objective function of (12), its value must remain approximately equal between simulations. Consequently, changing drainage amounts compensates for differences in root water uptake between 1-, 2-, and 3-D simulations. Most importantly, the standard deviation results in Table 4 shows that the spatial variation in drainage rate and root water uptake decreases

when reducing multidimensional soil water flow and root water uptake to decreasing spatial dimensions. This may have large implications for chemical transport in root zones, as drainage rates and corresponding chemical transport rates will vary according to root water uptake distribution.

Figure 10 presents a detailed two-dimensional contour plot of the spatial variability of cumulative flux density (mm) during the September 18–29 monitoring period at the 55 cm soil depth, as computed from the HYDRUS-3D model. Cumulative net soil water flow is downward (positive values), except for a small portion of the rooting zone domain at $(x, y) = (1.4, 2.5)$. Although the results in Figure 10 are influenced by the choice of the lower boundary condition, Figure 10 clearly demonstrates that the spatial variability of the drainage rate below the rooting zone is large, with values increasing as cor-
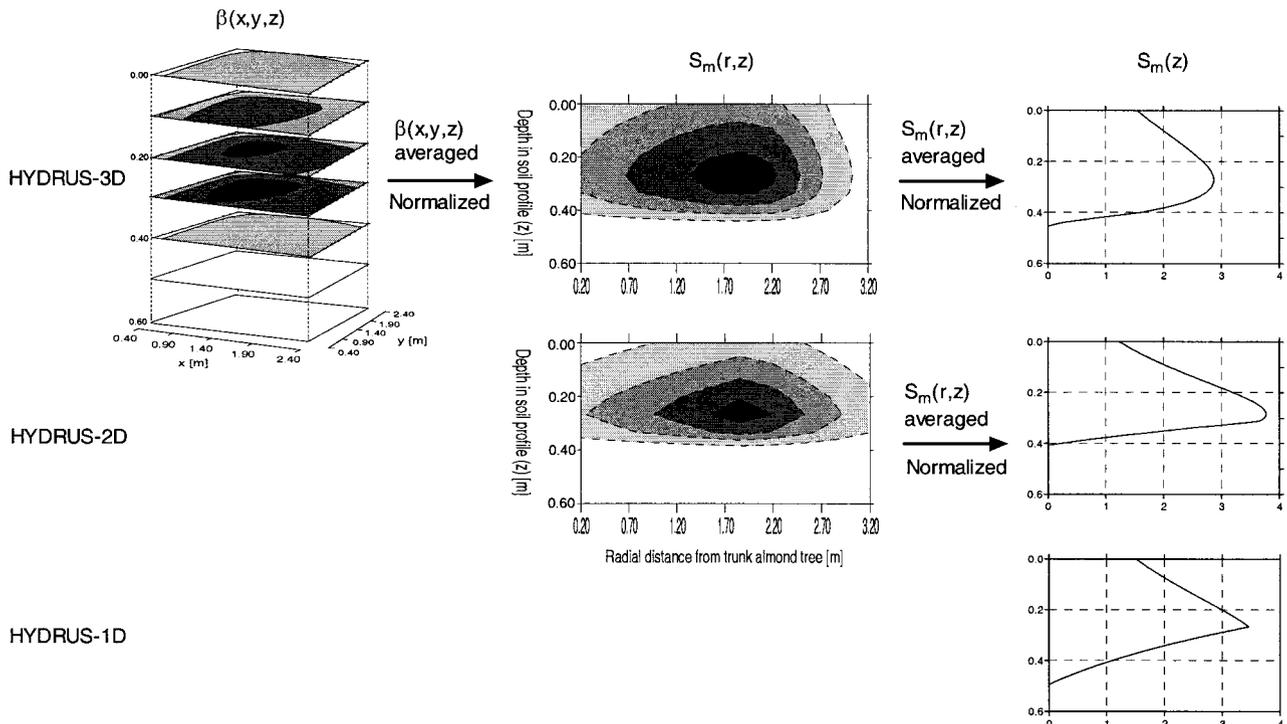

Figure 9. Comparison of optimized spatial distributions of potential root water uptake in one, two, and three dimensions.
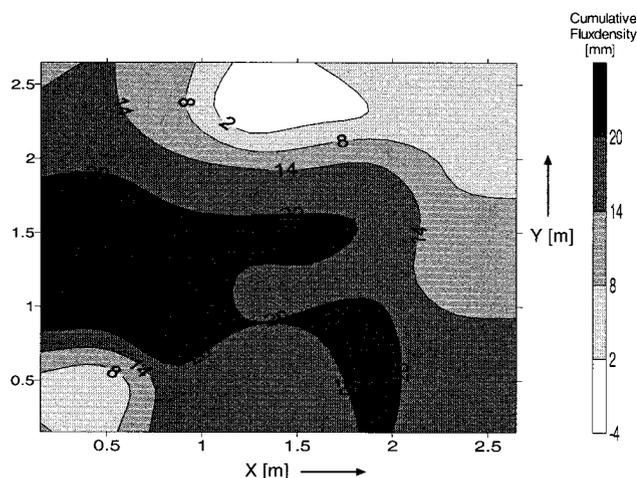
Figure 10. Two-dimensional contour plot of spatial variability in cumulative drainage at the 0.55 m soil depth during monitoring period.

responding root water uptake values decrease. The increasing accurate spatial description of root water uptake and soil water flow with increasing spatial dimension is essential to improve model predictions of water fluxes and contaminant transport through the vadose zone. Moreover, total chemical load to the groundwater will depend on local concentration and fluxes and their spatial variability. Specifically, although the average chemical load can be small, as computed from average flux and concentration values in one-dimensional simulations, the actual chemical load can be much larger. For example, this is the case if local regions of high drainage rates, as controlled by low root water uptake, correspond with high concentration values.

3.3. One-Dimensional Root Water Uptake Model in Multidimensional Flow Modeling

The final analysis investigates the need for a multidimensional root water uptake approach in multidimensional flow modeling. For this purpose, we compare simulation results when including a one-dimensional root water uptake model in the multidimensional water flow modeling. For this purpose the soil hydraulic parameters (h_{50}, n, and K_s) and root parameters (Z_m, p_z, and z^*) were taken from the optimized HYDRUS-1D model. The final fitting results are expressed by the RMSE and R^2 values between measured and simulated water content values. These values, combined with the water balance components, including their spatial variability as determined by standard deviation values, are presented in Table 5. As expected, correlations are low (R^2 values of ~0.6), and

Table 4. Components of the Soil Water Balance Using HYDRUS-1D, HYDRUS-2D, and HYDRUS-3D[a]

	HYDRUS-1D	HYDRUS-2D	HYDRUS-3D
T_{pot}, mm	48.70	48.70	48.70
E, mm	6.99	6.99	6.49
T_a, mm	42.04	36.53 (35.18)	39.45 (39.60)
Drainage, mm	7.78	8.62 (5.33)	13.06 (8.11)
Δ storage, mm	56.81	52.18	59.00

[a]Parentheses give standard deviation. Variables are cumulative potential almond transpiration T_{pot}, soil evaporation E, actual root water uptake T_a, drainage, and change in storage.

Table 5. Components of the Soil Water Balance (and Standard Deviation) Obtained Using One-Dimensional Root Water Uptake Model in Multidimensional Flow Model

	HYDRUS-2D	HYDRUS-3D
T_{pot}, mm	48.70	48.70
E, mm	6.99	6.25
T_a, mm	42.46 (37.48)	41.97 (38.02)
Drainage, mm	10.80 (4.58)	11.34 (6.44)
Δ storage, mm	60.25	59.57
RMSE, m^3 m^{-3}	0.0553	0.0627
R^2	0.61	0.57

RMSE values are large (0.05–0.06 m^3 m^{-3}), indicating that a one-dimensional root water uptake model is unable to capture soil moisture variations caused by spatially variable root water uptake. Moreover, whereas total root water uptake and its variation are almost identical to the comparable HYDRUS-1D values in Table 4, total drainage was increased and spatial variability decreased. The inability to predict within root zone soil moisture variability using a one-dimensional root water uptake model in multidimensional rooting systems clearly favors the need for multidimensional root water uptake and flow models, if detail at this scale is required.

4. Conclusions

In this paper, we have tested the suitability of a three-dimensional model for the simultaneous, dynamic simulation of soil water flow and root water uptake. After parameter optimization of the selected root water uptake model and soil hydraulic parameters, the agreement between simulated and measured water contents values during the 16 day period was good, with an overall time-averaged root mean squared error value of 0.018 m^3 m^{-3}. These results are excellent, bearing in mind that the standard error of the water content measurements was between 0.01 and 0.02 m^{-3} m^{-3}. Subsequently, using the same field data set of multidimensional volumetric water content values, the results of the three-dimensional root water uptake model were compared with inverse modeling data, describing root water uptake and soil water flow in two and one dimensions. Independently measured soil water retention data agreed favorably with the optimized retention curves using either one-, two-, or three-dimensional root water uptake with corresponding multidimensional water flow models. The high value of the optimized water stress parameter agreed with the low water holding capacity of the sandy field soil.

Optimized root water uptake distributions between one-, two-, and three-dimensional flow models with corresponding root water uptake models were almost identical. These results provide evidence that the presented spatial aggregation of soil moisture data is adequate for calibration purposes to arrive at effective root water uptake parameters. Also, when comparing water balance components between the three models, all models were in approximate agreement. However, major differences occurred for the spatial variation in root water uptake and drainage rates between one-dimensional and multidimensional models. This loss of information regarding variability of drainage rates and root water uptake clearly justifies the need for multidimensional root water uptake and flow models, especially when the fate and transport of chemicals below the rooting zone for single trees is of concern.

References

Andreu, L., J. W. Hopmans, and L. J. Schwankl, Spatial and temporal distribution of soil water balance for a drip-irrigated almond tree, *Agric. Water Manage.*, 35, 123–146, 1997.

Bäck, T., *Evolutionary Algorithms in Theory and Practice: Evolution Strategies, Evolutionary Programming, Genetic Algorithms*, Oxford Univ. Press, New York, 1996.

Canadell, J., R. B. Jackson, J. R. Ehleringer, H. A. Mooney, O. E. Sala, and E. D. Schulze, Maximum rooting depth of vegetation types at the global scale, *Oecologia*, 108, 583–595, 1996.

Celia, M. A., E. T. Bouloutas, and R. L. Zarba, A general mass-conservative numerical solution for the unsaturated flow equation, *Water Resour. Res.*, 26, 1483–1496, 1990.

Clausnitzer, V., and J. W. Hopmans, Simultaneous modeling of transient three-dimensional root growth and soil water flow, *Plant Soil*, 164, 299–314, 1994.

Clothier, B. E., and S. R. Green, Rootzone processes and the efficient use of irrigation water, *Agric. Water Manage.*, 25, 1–12, 1994.

Coelho, F. E., and D. Or, A parametric model for two-dimensional water uptake intensity by corn roots under drip irrigation, *Soil Sci. Soc. Am. J.*, 60, 1039–1049, 1996.

Duan, Q., S. Sorooshian, and V. Gupta, Effective and efficient global optimization for conceptual rainfall-runoff models, *Water Resour. Res.*, 28, 1015–1031, 1992.

Feddes, R. A., P. Kowalik, K. Kolinska-Malinka, and H. Zaradny, Simulation of field water uptake by plants using a soil water dependent root extraction function, *J. Hydrol.*, 31, 13–26, 1976.

Gardner, W. R., Dynamic aspects of water availability to plants, *Soil Sci.*, 89, 63–73, 1960.

Gardner, W. R., Relation of root distribution to water uptake and availability, *Agron. J.*, 56, 41–45, 1964.

Gardner, W. R., Dynamic aspects of soil-water availability to plants, *Annu. Rev. Plant Physiol.*, 16, 323–342, 1965.

Gardner, W. R., and C. F. Ehlig, Some observations on water movement to plant roots, *Agron. J.*, 54, 453–456, 1962.

Golden Software, version 6.04c, Golden, Colorado, 1996.

Green, S., and B. Clothier, The root zone dynamics of water uptake by a mature apple tree, *Plant Soil*, 206, 61–77, 1999.

Holland, J. H., *Adaptation in Natural and Artificial Systems: An Introductory Analysis With Applications to Biology, Control, and Artificial Intelligence*, Univ. of Mich. Press, Ann Arbor, 1975.

Homaee, M., Root water uptake under non-uniform transient salinity and water stress, Ph.D. thesis, pp. 169, Agric. Univ. Wageningen, Wageningen, Netherlands, 1999.

Inoue, M., J. Šimůnek, J. W. Hopmans, and V. Clausnitzer, In situ estimation of soil hydraulic functions using a multistep soil-water extraction technique, *Water Resour. Res.*, 34, 1035–1050, 1998.

Inoue, M., J. Šimůnek, J. S. Shiozawa, and J. W. Hopmans, Simultaneous estimation of soil hydraulic and solute transport parameters from transient infiltration experiments, *Adv. Water Resour.*, 23(7), 677–688, 2000.

Jarvis, N. J., A simple empirical model of root water uptake, *J. Hydrol.*, 107, 57–72, 1989.

Kool, J. B., and J. C. Parker, Analysis of the inverse problem for transient unsaturated flow, *Water Resour. Res.*, 24, 817–830, 1988.

Koumanov, K. S., J. W. Hopmans, L. J. Schwankl, L. Andreu, and A. Tuli, Application efficiency of micro-sprinkler irrigation of almond trees, *Agric. Water Manage.*, 34, 247–263, 1997.

Molz, F. J., Models of water transport in the soil-plant system: A review, *Water Resour. Res.*, 17, 1245–1260, 1981.

Molz, F. J., and I. Remson, Extraction term models of soil moisture use by transpiring plants, *Water Resour. Res.*, 6, 1346–1356, 1970.

Mualem, Y., A new model for predicting the hydraulic conductivity of unsaturated porous media, *Water Resour. Res.*, 12, 513–522, 1976.

Musters, P. A. D., and W. Bouten, Assessing rooting depths of an Austrian pine stand by inverse modeling soil water content maps, *Water Resour. Res.*, 35, 3041–3048, 1999.

Neuman, S. P., R. A. Feddes, and E. Bresler, Finite element analysis of two-dimensional flow in soil considering water uptake by roots, I, Theory, *Soil Sci. Soc. Am. J.*, 35, 224–230, 1975.

Nyer, E. K., and E. G. Gatliff, Phytoremediation, *Ground Water Monit. Rem.*, 16(1), 58–62, 1996.

Penny, J., and G. Lindfield, *Numerical Methods Using MATLAB*, 328 pp., Ellis Horwood, Chichester, England, 1995.

Raats, P. A. C., Steady flows of water and salt in uniform soil profiles with plant roots, *Soil Sci. Soc. Am. Proc.*, 38, 717–722, 1974.

Ritchie, J. T., Model for predicting evaporation from a row crop with incomplete cover, *Water Resour. Res.*, 8, 1204–1213, 1972.

Šimůnek, J., and J. W. Hopmans, Parameter optimization and nonlinear fitting, in *Methods of Soil Analysis*, *Part I*, 3rd ed., *Monogr. 9*, edited by G. C. Topp and J. H. Dane, Am. Soc. of Agron., Madison, Wis., in press, 2001.

Šimůnek, J., K. Huang, and M. T. van Genuchten, The SWMS_3D code for simulating water flow and solute transport in three-dimensional variably saturated media, Version 1.2, *Res. Rep. 139*, 155 pp., U.S. Salinity Lab., U.S. Dep. of Agric., Agric. Res. Serv., Riverside, Calif., 1995.

Šimůnek, J., M. Šejna, and M. T. van Genuchten, The HYDRUS-1D software package for simulating the one-dimensional movement of water, heat, and multiple solutes in variably-saturated media, Version 2.0, 202 pp., *Rep. IGWMC-TPS-70*, Int. Ground Water Model. Cent., Colo. Sch. of Mines, Golden, 1998.

Šimůnek, J., M. Šejna, and M. T. van Genuchten, The HYDRUS-2D software package for simulating two-dimensional movement of water, heat, and multiple solutes in variably saturated media, Version 2.0, *Rep. IGWMC-TPS-53*, 251 pp., Int. Ground Water Model. Cent., Colo. Sch. of Mines, Golden, 1999.

Snyder, R. L., and W. O. Pruitt, Crop coefficients, in *Irrigation Scheduling—A Guide for Efficient On-Farm Water Management*, edited by D. A. Goldhamer and R. L. Snyder, *Pub. 21454*, 67 pp., Univ. of Calif. Div. of Agric. and Nat. Resour., Davis, 1988.

Snyder, R. L., D. W. Henderson, W. O. Pruitt, and A. Dong, California irrigation management information system final report, vol. I, Dep. of Land, Air, and Water Resour., Univ. of Calif., Davis, 1985.

Somma, F., J. W. Hopmans, and V. Clausnitzer, Transient three-dimensional modeling of soil water and solute transport with simultaneous root growth, root water, and nutrient uptake, *Plant Soil*, 202, 281–293, 1998.

The MathWorks, MATLAB, version 5.3, MathWorks, Natick, Mass., 1999.

Van Genuchten, M. T., A closed-form equation for predicting the hydraulic conductivity of unsaturated soils, *Soil Sci. Soc. Am. J.*, 44, 892–898, 1980.

Van Genuchten, M. T., A numerical model for water and solute movement in and below the root zone, *Res. Rep. 121*, U.S. Salinity Lab., Agric. Res. Serv., U.S. Dep. of Agric., Riverside, Calif., 1987.

Van Genuchten, M. T., and S. K. Gupta, A reassessment of the crop tolerance response function, *Bull. Indian Soc. Soil Sci.*, 4, 730–737, 1993.

Vrugt, J. A., W. Bouten, and A. H. Weerts, Information content of data for identifying soil hydraulic parameters from outflow experiments, *Soil Sci. Soc. Am. J.*, 65, 19–27, 2001a.

Vrugt, J. A., J. W. Hopmans, and J. Šimunek, Calibration of a two-dimensional root water uptake model for a sprinkler-irrigated almond tree, *Soil Sci. Soc. Am. J.*, in press, 2001b.

Walton, B. T., and T. A. Anderson, Microbial degradation of trichloroethylene in the rhizosphere: Potential application to biological remediation of waste sites, *Appl. Environ. Microbiol.*, 56, 1012–1016, 1990.

Wang, Q. J., The genetic algorithm and its application to calibrating conceptual rainfall-runoff models, *Water Resour. Res.*, 27, 2467–2471, 1991.

Warrick, A. W., D. O. Lomen, and A. A. Fard, Linearized moisture flow with root extraction for three dimensional, steady conditions, *Soil Sci. Soc. Am. J.*, 44, 911–914, 1980.

Whisler, F. D., A. Klute, and R. J. Millington, Analysis of steady state evapotranspiration from a soil column, *Soil Sci. Soc. Am. Proc.*, 32, 167–174, 1968.

J. W. Hopmans, Hydrology Department, Department of Land, Air and Water, University of California, 1 Shields Avenue, 123 Veihmeyer Hall, Davis, CA 95616, USA. (jwhopmans@ucdavis.edu)

J. Šimunek, USDA Salinity Laboratory, University of California, Riverside, CA 95207, USA.

M. T. van Wijk and J. A. Vrugt, Institute for Biodiversity and Ecosystem Dynamics, University of Amsterdam, Nieuwe Achtergracht 166, Amsterdam 1018 WV, Netherlands.